Research Square

Preprints are preliminary reports that have not undergone peer review.
They should not be considered conclusive, used to inform clinical practice,
or referenced by the media as validated information.

Oxygen-Assisted Truncation of Coarse-Grained Electroplated CBN Grinding Wheels for Ultra-Smooth Grinding of Bearing Steel

Qiushi Li

232d9287@st.kumamoto-u.ac.jp

Kumamoto University: Kumamoto Daigaku https://orcid.org/0009-0000-3449-748X

Akihisa Kubota

Kumamoto University: Kumamoto Daigaku

Mitsuru Murai

Kumamoto University: Kumamoto Daigaku

Koji Kawamura

Kumamoto Industrial Research Institute

Research Article

Keywords: coarse-grained electroplated CBN wheel, oxygen-assisted truncation, end-face grinding, bearing steel, surface roughness

Posted Date: August 31st, 2026

DOI: https://doi.org/10.21203/rs.3.rs-10760206/v1

License: This work is licensed under a Creative Commons Attribution 4.0 International License.
Read Full License

Oxygen-Assisted Truncation of Coarse-Grained Electroplated CBN Grinding Wheels for Ultra-Smooth Grinding of Bearing Steel

Qiushi Li [a], Akihisa Kubota[a*], Mitsuru Murai[a,b], Koji Kawamura[b]

[a]Kumamoto University, 2-39-1 Kurokami, Chuo-ku, Kumamoto 860-8555, Japan

[b]Kumamoto Industrial Research Institute, 3-11-38 Higashimachi, Higashi-ku, Kumamoto 862-0901, Japan

*Corresponding author: kubota@mech.kumamoto-u.ac.jp

Highlights

- Oxygen supply accelerated grain-tip truncation of electroplated CBN wheels.
- Wear-debris analysis supported the oxidative removal of CBN against quartz glass.
- A truncated #120 CBN wheel achieved a surface roughness of Sa = 3.149 nm.
- A smooth bearing-steel surface was maintained at a depth of cut of 500 μm.
- An appropriate truncation extent is essential for generating a stable surface

Abstract

Coarse-grained electroplated cubic boron nitride (CBN) grinding wheels offer high material removal capability and long tool life, but non-uniform abrasive protrusion heights can generate deep grooves, limiting their use in precision finishing. This study investigated an oxygen-assisted truncation process for forming flattened cutting edges on coarse-grained electroplated CBN wheels and evaluated its application in end-face ultra-smooth grinding. Friction tests between polycrystalline CBN (PCBN) and quartz glass produced B- and O-rich wear debris with elemental distributions consistent with the oxidative removal of CBN. Under the tested conditions, supplemental oxygen increased the measured grain-tip truncation area ratio from 2.91% to 4.08% and the grain-tip removal height from 19.045 μm to 24.079 μm. When a truncated #120 wheel was applied to GCr15 bearing steel at a feed per revolution of 3 μm/rev, no distinct grinding grooves were observed and an Sa of 3.149 nm was achieved. Sa remained below 10 nm at nominal depths of cut ranging from 1 to 15 μm; even at a nominal depth of cut of 500 μm, Sa and Sz were 10.555 nm and 71.433 nm, respectively. Among the wheels tested, the wheel with a truncation area ratio of 2.91% produced the lowest mean Sa, whereas larger area ratios were accompanied by higher grinding forces and roughness values. These results demonstrate the feasibility of combining oxygen-assisted wheel truncation with end-face grinding to generate nanometer-scale surfaces using a coarse-grained electroplated CBN wheel; however, the truncation extent should be appropriately controlled to balance the surface finish and grinding force.

Keywords: coarse-grained electroplated CBN wheel; oxygen-assisted truncation; end-face grinding; bearing steel; surface roughness

1. Introduction

Hardened steel components, particularly bearing steel components, are widely used in bearings, precision transmission systems, dies, and molds. Their surface topography directly affects friction, wear, and rolling contact fatigue life [1-3], and is therefore a critical manufacturing attribute. Nanometer-scale surface finishes are commonly produced by multistep precision grinding, lapping, polishing, and superfinishing [4, 5]. Although these methods can produce high-quality surfaces, they often require long processing times and incur high costs.

Grinding with ultrafine-grit wheels offers an efficient finishing route; however, the limited chip space of these wheels promotes loading and necessitates frequent truing and dressing as abrasive-grain wear and wheel topography deterioration progress [6, 7]. In contrast, coarse-grained electroplated CBN wheels provide greater chip accommodation, high grain-retention strength, and low wheel wear, making them attractive for efficient machining [8, 9]. However, their use in precision finishing is limited by the random distributions of grain protrusion height, cutting-edge geometry, orientation, and position, which generate non-uniform grooves and degrade the finished surface [8, 10]. If the most protruding grain tips can be flattened and aligned near a common height while retaining an open wheel topography, coarse-grained wheels may combine a high material-removal capability with precision surface generation.

This concept requires the controlled truncation of protruding CBN grains. Previous studies have investigated the mechanical, laser, and ultrasonic truing of CBN wheels [11-15]. However, to the best of the authors' knowledge, no process has yet been established that precisely truncates a coarse-grained electroplated CBN wheel, quantitatively characterizes the resulting flat-tip topography, and directly applies the truncated wheel to generate workpiece surfaces with nanometer-scale roughness. Li et al. developed a quartz-based polishing method for the precise truncation of coarse-grained electroplated diamond wheels [16]; however, this study focused on diamond wheels and did not evaluate the truncated wheels during grinding. Touge et al. reported

that CBN can be removed by friction against quartz glass and proposed oxidative removal as a possible mechanism [17]. The effect of supplemental oxygen on the truncation of an electroplated CBN wheel and the impact of the resulting truncation extent on grinding performance remain unclear.

The surface generation principle used in this study is based on the overlap of successive paths traced by flattened grain tips. For an idealized grain with a flat-tip width w_n, successive grain paths overlap when the feed per revolution $f_{Gn}$is smaller than $w_n(f_{Gn} < w_n)$, thereby reducing the residual ridges formed between successive passes [18-20]. However, this condition alone is insufficient if sharp, untruncated grains remain dominant on the wheel end face. Therefore, ultra-smooth grinding requires both a sufficiently small feed per revolution and a controlled population of approximately coplanar truncated grains. Consequently, the grinding performance should be evaluated as a coupled function of the feed per revolution, nominal depth of cut, and truncation extent.

Accordingly, this study investigates the oxygen-assisted truncation of a coarse-grained electroplated CBN wheel and its application to end-face ultra-smooth grinding of GCr15 bearing steel. Friction experiments between a polycrystalline cubic boron nitride (PCBN) plate and quartz glass were first conducted to examine the elemental characteristics of the wear debris generated during the CBN removal. Wheel truncation experiments were performed to quantify the changes in grain-tip removal height and truncation area ratio associated with supplemental oxygen. Finally, grinding experiments were conducted to examine the effects of the feed per revolution, nominal depth of cut, and truncation extent on the surface roughness and grinding force. This experimental sequence links elemental evidence consistent with oxidative CBN removal, oxygen-assisted modification of grain-tip topography, and the resulting surface generation performance.

2. Materials and methods

2.1. PCBN model experiment and CBN-wheel truncation

To examine CBN removal, friction experiments were conducted between a PCBN plate used as a model specimen and a synthetic quartz glass plate. This approach was based on previous observations of diamond removal by friction against quartz glass. The elemental characteristics of CBN removal were examined by analyzing the composition of the wear debris. Fig. 1(a) shows the PCBN plate mounted onto the specimen holder. The PCBN contained 90 wt.% CBN, limiting the contribution of the binder phase to the debris analysis. A fluororubber pad was inserted between the specimen holder and the PCBN plate to improve contact with the quartz glass polishing plate, and the components were bonded with an adhesive. Fig. 1(b) shows the CBN grinding wheel used in the truncation and grinding experiments. The wheel had an outer diameter of 15 mm, bore diameter of approximately 10 mm, and a grit size of #120. Oxygen was supplied near the contact region during the selected wheel truncation tests to examine its influence on CBN removal and wheel truncation.

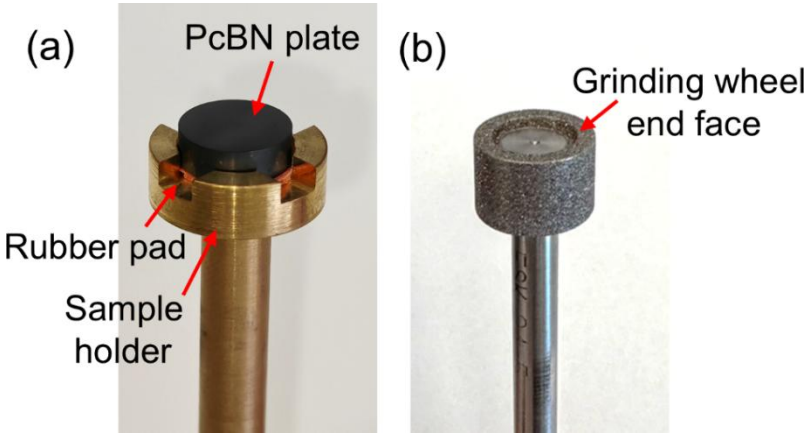


Fig. 1. Experimental specimens: (a) PCBN plate mounted on the sample holder and (b) #120 electroplated CBN grinding wheel.

Fig. 2 schematically illustrates the fundamental concept of grain-tip truncation for the #120 electroplated CBN grinding wheel, as shown in Fig. 1(b). In a coarse-grained

wheel, CBN grains with different sizes, shapes, orientations, and protrusion heights are distributed on the wheel surface. The sharp tips of the most protruding grains generated grooves of nonuniform depth, thereby degrading the finished-surface quality. Truncation selectively removes the protruding portions of these grain tips, reduces the variation in the active grain-tip height, and forms locally flat cutting edges that are aligned closer to a common plane. This modification is expected to suppress the formation of deep grooves while preserving the open topography and chip accommodation capability of the coarse-grained wheel. However, the extreme hardness and chemical stability of CBN make the controlled removal of grain tips and the formation of approximately coplanar flat cutting edges challenging.

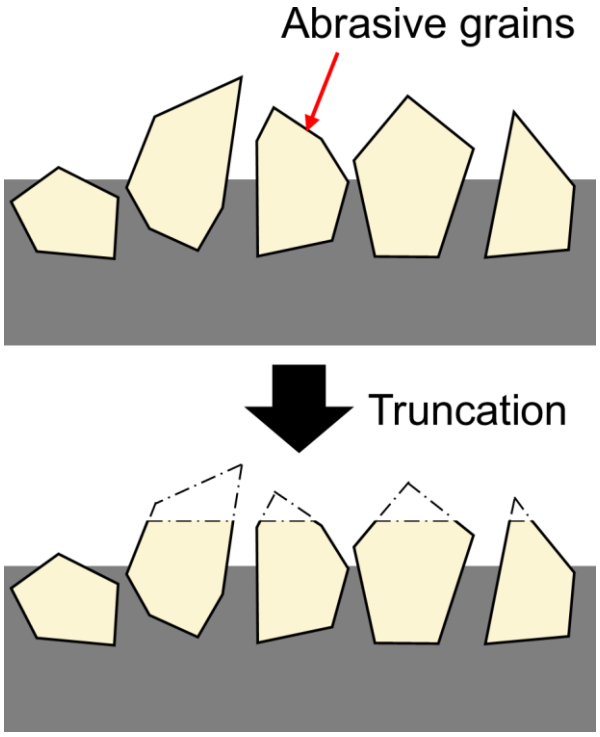


Fig. 2. Schematic of the grinding wheel truncation.

Fig. 3(a) shows a photograph of the experimental apparatus, and Fig. 3(b) schematically illustrates the contact configuration and oxygen supply arrangement. In the PCBN model experiments, the PCBN specimen holder was mounted on the spindle, whereas in the wheel-truncation experiments, the electroplated CBN wheel was mounted directly on the spindle. In both experiments, the PCBN specimen or CBN

wheel was pressed against the quartz-glass polishing plate under a prescribed load to establish frictional contact. Because oxidative CBN removal during friction against quartz glass has been proposed previously [17], an oxygen-supply nozzle was positioned adjacent to the contact interface. This configuration was used to investigate the influence of supplemental oxygen on CBN removal and grain-tip truncation.

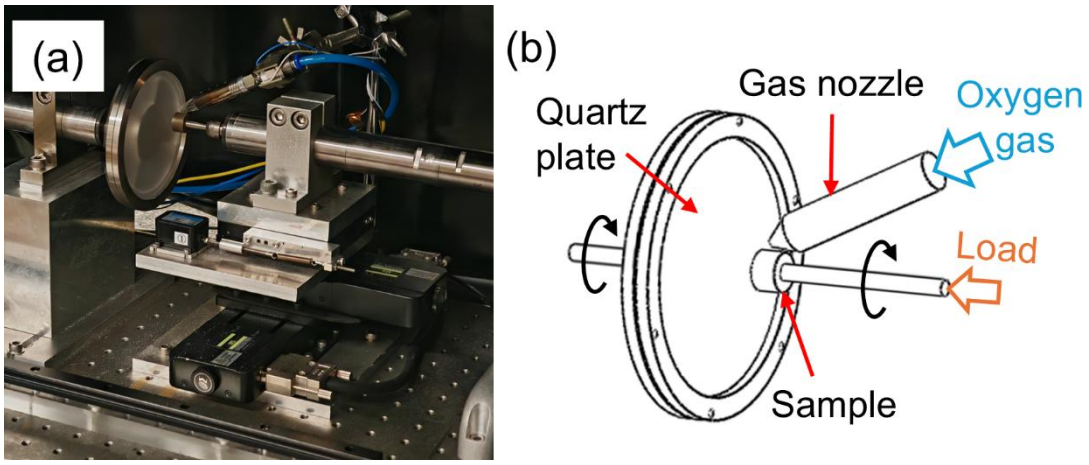


Fig. 3. Experimental setup for oxygen-assisted frictional truncation: (a) photograph of the setup, and (b) schematic illustration of the oxygen supply to the quartz–sample contact interface.

Table 1 summarizes the experimental conditions for the PCBN friction test. The rotational speed and applied load were selected to generate a sufficient quantity of wear debris for subsequent elemental analysis. Immediately after the test, the PCBN specimen and its holder were immersed in acetone in an evaporating dish and ultrasonically cleaned for 1 min to detach and collect the wear debris adhering to the specimen and holder. The resulting acetone suspension was then heated under continuous ultrasonic agitation until the acetone completely evaporated. Finally, the residual wear debris was collected from the evaporating dish using adhesive carbon tape for subsequent observation and elemental analysis.

Table 1 PCBN polishing conditions

Sample	PCBN plate, φ9.525 mm, 90 wt.% CBN
Polishing plate	Synthetic quartz plate, φ100 mm
Load	5 N
Sample rotational speed	1000 min^{-1}
Quartz rotational speed	1000 min^{-1}
Contact radius	40 mm
Relative speed	~5.2 m/s
Processing time	60 min

Table 2 summarizes the experimental conditions for the end-face truncation of the electroplated CBN wheels. First, an exploratory sequential test was conducted using a single wheel to characterize the evolution of grain-tip truncation under progressively increasing oxygen flow rates. The wheel was initially processed in ambient air without supplemental oxygen and was subsequently processed with oxygen supplied at flow rates of 2.5, 5.0, 7.5, and 10.0 L/min. Each condition was applied for 15 min, and the change in grain protrusion height was measured after each processing stage using a laser scanning microscope (OLS4100, Olympus). Because all conditions were applied sequentially to the same wheel, the effects of oxygen flow rate, cumulative processing time, and the evolving wheel topography were inherently confounded. Therefore, these results characterize the evolution of truncation under the specified test sequence and should not be interpreted as statistically independent comparisons among the oxygen flow rates.

Separate air-and oxygen truncation tests were conducted for 40 min to compare the resulting grain-tip topographies under a fixed processing time. One wheel was truncated in ambient air, and the other was truncated with oxygen supplied at 7.5 L/min under otherwise identical conditions. The wheel end faces were examined before and after truncation using a differential interference contrast optical microscope (STM6-LM, Olympus) and a laser scanning microscope (OLS4100, Olympus). The resulting images and three-dimensional topographies were used to determine the grain-tip truncation

area ratio and the grain-tip removal height, respectively. Because only one wheel was tested under each gas condition, these results were treated as descriptive comparisons under the specified conditions.

For the mass loss measurements, another pair of CBN wheels was truncated for 120 min: one in ambient air and the other with oxygen supplied at 7.5 L/min. The masses of each wheel and its corresponding quartz-glass polishing plate were measured before and after truncation using an electronic balance (GH-252, A&D). The relative wheel-to-quartz mass-loss ratios obtained under the two gas conditions were then compared. Because only one wheel–plate pair was tested under each condition, this comparison was limited to the specimens and conditions examined in this study.

Table 2 Experimental conditions for end-face truncation of electroplated CBN wheels

Sample	Electroplated CBN wheel, φ15 mm, #120 grit
Polishing plate	Synthetic quartz plate, φ100 mm
Load	1 N
Sample rotational speed	250 min^{-1}
Quartz-plate rotational speed	250 min^{-1}
Contact radius	40 mm
Relative speed	~1.0 m/s
Atmosphere	Air or oxygen flow
Gas flow rate	0–10 L/min

2.2. Principle and conditions of end-face ultra-smooth grinding

Fig. 4 illustrates the fundamental concept of end-face ultra-smooth grinding. As shown in Fig. 4(a), the wheel rotates while simultaneously advancing relative to the workpiece in the feed direction. During one wheel revolution, the trajectory of a given abrasive grain is displaced in the feed direction by the feed per revolution, f_{Gn}. Fig. 4(b) illustrates the idealized surface-generation process associated with a single truncated grain. When the grain tip has an effective flat-tip width, w_n in the feed

direction, it generates a locally flat grinding track. During the subsequent wheel revolution, the trajectory of the same grain is laterally displaced by (f_{Gn}). When ($f_{Gn} < w_n$), successive grinding tracks overlap, thereby suppressing the formation of feed-periodic residual ridges between adjacent passes. However, in an actual grinding wheel, the generated surface also depends on the distributions of flat-tip width, grain protrusion height, and grain position. Therefore, the track-overlap condition represents a fundamental geometric criterion for ultra-smooth surface generation but is not, by itself, a sufficient condition.

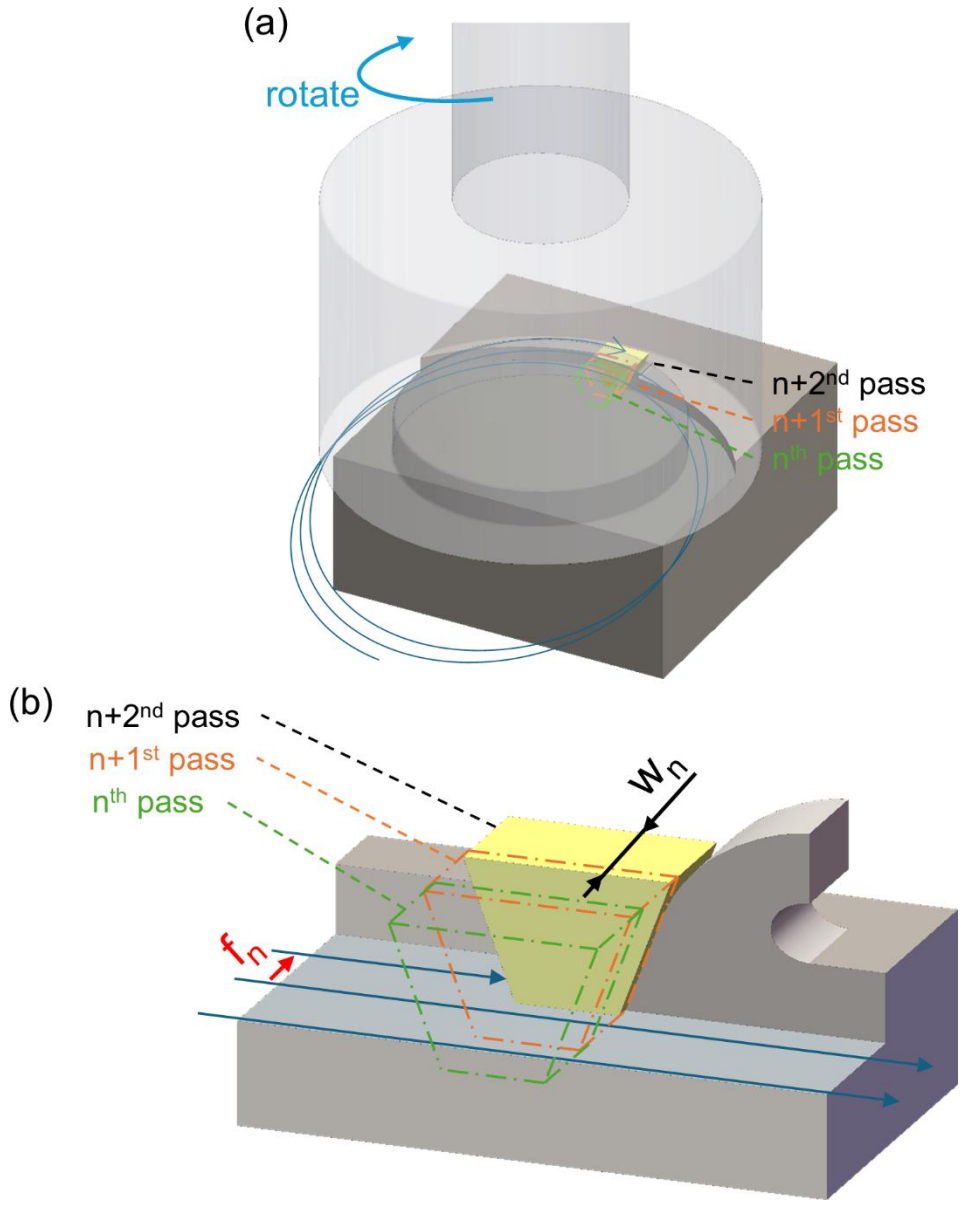


Fig. 4. Principle of end-face ultra-smooth grinding using a truncated abrasive grain: (a) trajectory of an abrasive grain resulting from wheel rotation and feed, and (b) surface generation when the feed per revolution is smaller than the width of the flattened grain tip

Fig. 5(a) shows the experimental setup used for the grinding tests, which were conducted on a three-axis CNC machine (V33i, Makino Milling Machine Co., Ltd.). The workpiece was clamped in a vise mounted on a multicomponent dynamometer (9129A, Kistler) to measure the grinding force. Fig. 5(b) illustrates the grinding

configuration and principal process parameters. The wheel rotational speed was fixed at 10,000 min^{-1} throughout all grinding tests. An emulsifiable grinding fluid (B-Cool MC 660, Blaser Swisslube) diluted to 7 vol% was used in all grinding tests.

First, the effect of feed per revolution was investigated using a single truncated wheel. The feed rate was varied from 30 to 500 mm/min, corresponding to feed-per-revolution values of 3–50 μm/rev, while the nominal depth of cut was maintained at 1 μm. In a separate experiment, the grinding performance of an untreated wheel was compared with that of a separately prepared truncated wheel under identical conditions: a feed rate of 30 mm/min (3 μm/rev) and a nominal depth of cut of 1 μm. Subsequently, the effect of the nominal depth of cut was investigated using the same truncated wheel employed in the feed-per-revolution tests. The nominal depth of cut was varied from 1 to 15 μm, while the feed rate was maintained at 30 mm/min. An additional test was conducted using the same wheel at a nominal depth of cut of 500 μm under the same wheel speed and feed rate conditions. After grinding, the workpieces were ultrasonically cleaned in acetone, and the ground surfaces were characterized using a scanning white-light interferometric optical profiler (SWLI; NewView 7300, ZYGO).

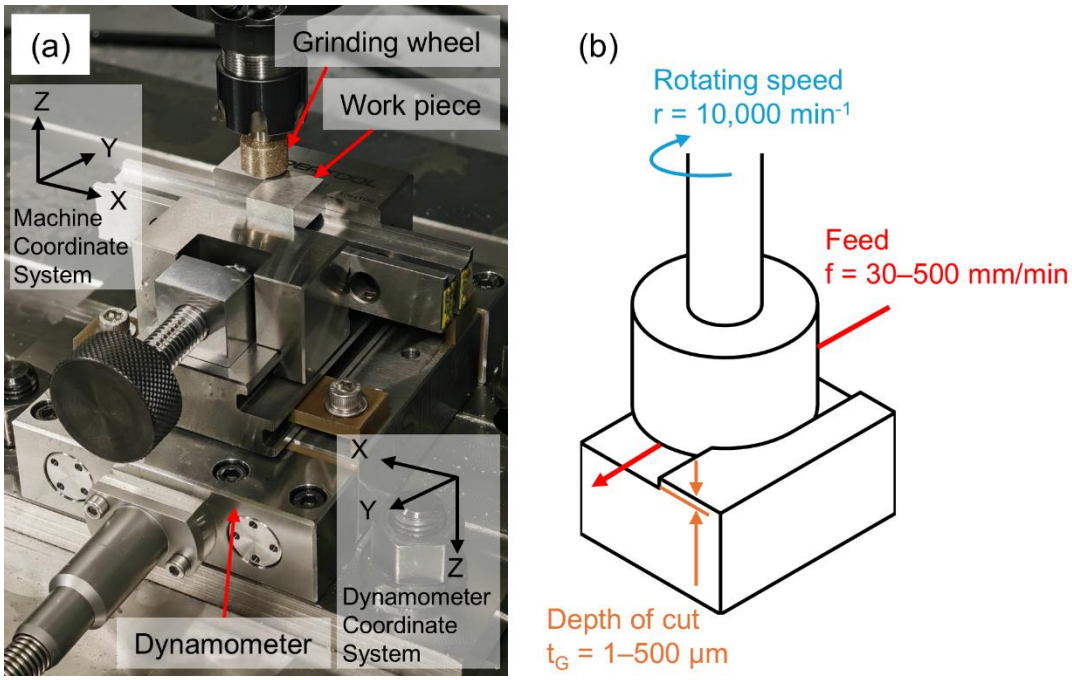


Fig. 5. Experimental setup and grinding parameters: (a) photograph of the grinding setup showing the grinding wheel, workpiece, and dynamometer, and (b) schematic illustration of the grinding configuration showing the spindle speed, feed rate, and depth of cut.

3. Results and discussion

3.1. Elemental and removal characteristics associated with oxygen-assisted CBN removal

Fig. 6 shows the electron probe microanalysis (EPMA) results for the wear debris generated by the friction between the PCBN plate and quartz glass polishing plate. Fig. 6(a) shows the secondary electron image, and Fig. 6(b) shows the composition image of the same area. The elemental maps in Figs. 6(c)–(f) reveal that the right-hand region of the analyzed area was enriched in Si and O and was therefore attributed primarily to debris originating from the quartz glass polishing plate. In contrast, the B-rich region did not overlap with the Si-rich region but showed a clear spatial correspondence with the O-rich region. A relatively weak N signal was also observed in this region. These

elemental distributions suggest that the boron-containing wear debris was associated with oxygen. However, EPMA cannot identify the chemical state or crystalline phase of the debris. Therefore, the formation of specific boron oxides could not be confirmed. Nevertheless, the observed spatial distributions of B, N, and O are consistent with the oxidative CBN removal mechanism proposed by Touge et al. [17].

The PCBN experiment was used as a model system to examine the elemental characteristics associated with tribochemical CBN removal. Compared with the direct analysis of individual grains on an electroplated CBN wheel, the high CBN content and continuous contact surface of the PCBN specimen were intended to reduce the influence of variations in grain shape, protrusion height, and the metallic bond layer. However, a possible contribution from the PCBN binder phase to the wear debris cannot be completely excluded. Accordingly, the EPMA results were used only to evaluate whether the elemental characteristics of the wear debris were consistent with oxidative CBN removal; they neither identified the reaction products nor established a specific reaction pathway. Subsequent wheel-truncation experiments were conducted to determine whether supplemental oxygen was associated with increased wheel mass loss and a greater measured extent of grain-tip truncation in actual electroplated CBN wheels.

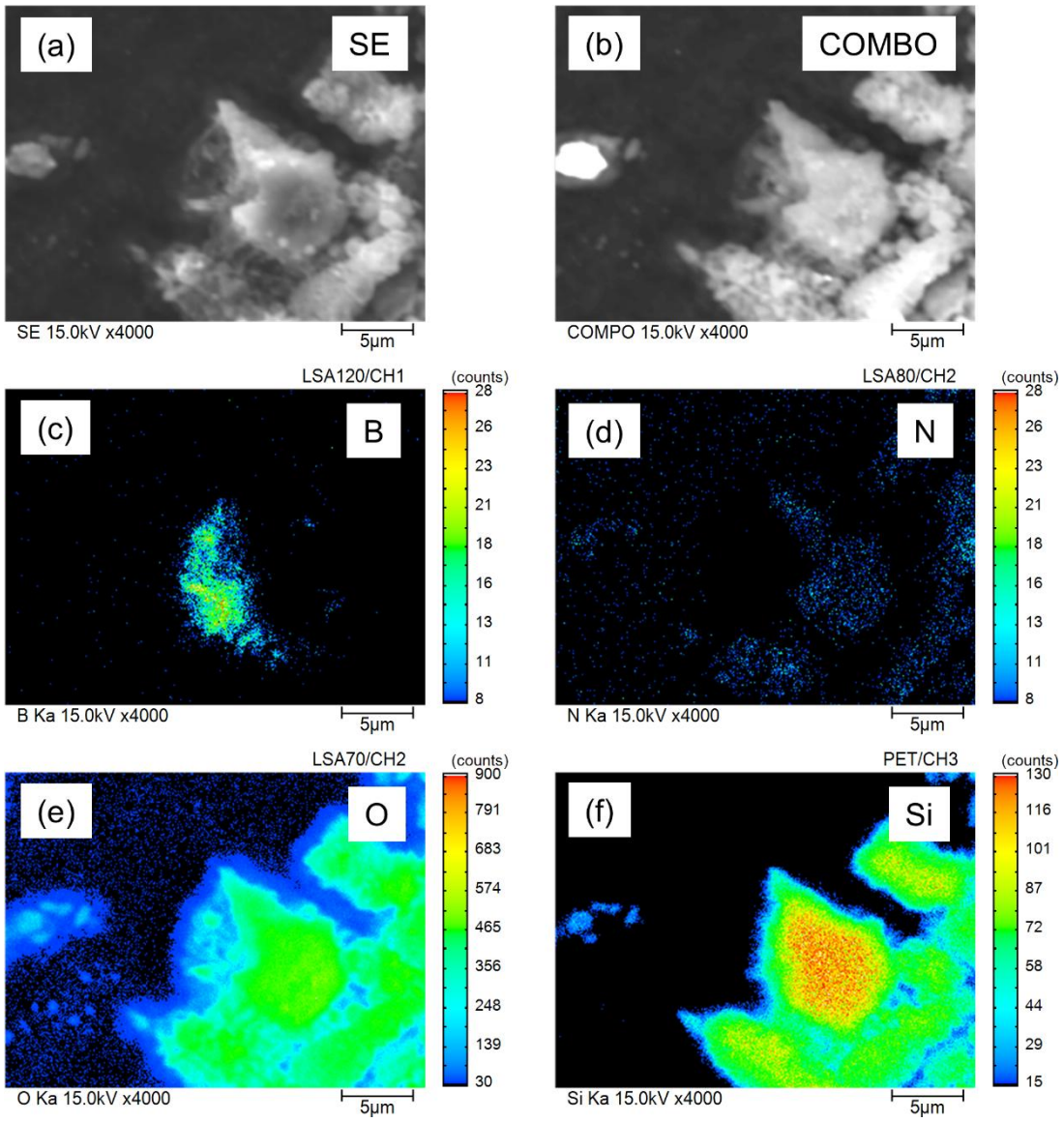


Fig. 6. EPMA analysis of wear debris generated during dry friction between a PCBN plate and quartz glass polishing plate: (a) secondary electron (SE) image, (b) COMPO image, and elemental maps of (c) boron, (d) nitrogen, (e) oxygen, and (f) silicon.

Fig. 7 compares the relative wheel-to-quartz mass-loss ratios obtained after wheel truncation in ambient air and with the supplemental oxygen. For each gas condition, the CBN wheel and its corresponding quartz glass polishing plate were weighed before and after truncation using an electronic balance. The wheel mass loss, Δm_{wheel}, and quartz-glass mass loss, Δm_{quartz}, were calculated from the respective differences

between the masses measured before and after truncation. To normalize the wheel mass loss by the concurrent wear of the quartz-glass plate, the relative wheel-to-quartz mass-loss ratio, $\eta_{W/Q}$, is defined as follows:

$$\eta_{W/Q} = \frac{\Delta m_{wheel}}{\Delta m_{quartz}} \times 100\% \quad (1)$$

Under both gas conditions, the mass loss of the CBN wheel was less than that of the corresponding quartz-glass polishing plate. The relative wheel-to-quartz mass-loss ratio increased from 0.698% in ambient air to 3.424% with supplemental oxygen; thus, the value obtained with supplemental oxygen was approximately 4.9 times that obtained in ambient air. However, because only one wheel–plate pair was tested under each gas condition, this difference should be interpreted as a descriptive comparison between the tested specimens rather than as a statistically validated effect of oxygen. Nevertheless, the direction of the change was consistent with the larger grain-tip removal height and truncation area ratio measured with supplemental oxygen in the separate wheel-topography experiments.

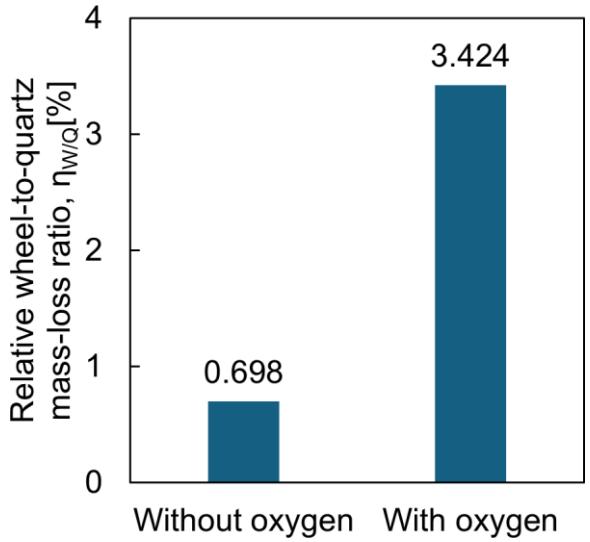


Fig. 7. Relative wheel-to-quartz mass-loss ratios measured after wheel truncation in ambient air and with supplemental oxygen.

Fig. 8 shows the abrasive-grain height reduction measured during successive 15 min

truncation intervals in ambient air and with oxygen supplied at flow rates ranging from 2.5 to 10 L/min. Because the processing time was identical for each interval, the increase in grain-height reduction with increasing oxygen flow rate suggests an apparent positive dependence of the truncation efficiency on oxygen flow rate. This tendency is consistent with enhanced CBN removal at greater oxygen availability near the contact interface. However, because the oxygen flow rates were applied successively to the same wheel in ascending order, oxygen flow rate was unavoidably confounded with cumulative processing time and the evolution of the wheel topography. Therefore, the results suggest, but do not independently establish, a flow-rate-dependent enhancement of CBN grain-tip truncation. The separate air-versus-oxygen comparisons shown in Figs. 7, 9, and 10 further support the overall enhancement of CBN removal and grain-tip truncation by supplemental oxygen under the tested conditions.

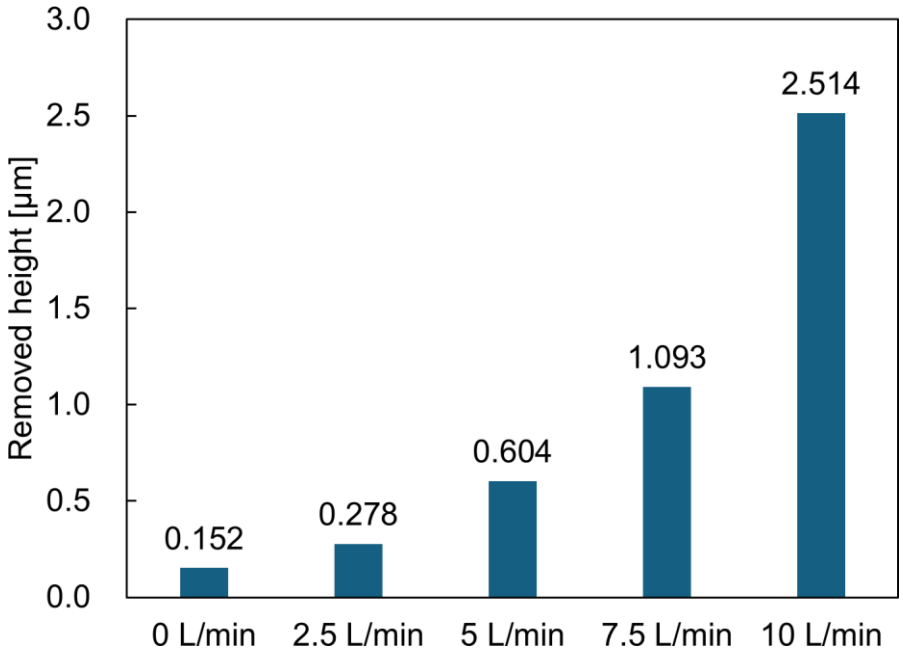


Fig. 8. Evolution of abrasive-grain height reduction during sequential truncation in ambient air and with increasing oxygen flow rates.

3.2. Quantification of CBN-wheel truncation

Differential interference contrast (DIC) microscopy revealed that the flat grain-tip regions formed by truncation were bright blue areas with relatively uniform contrast. These regions were extracted from the DIC images and converted into binary masks using image-processing software. The grain-tip truncation area ratio was defined as the total projected area of the extracted flat-tip regions divided by the total analyzed area of the active wheel end face. The truncation area ratio was calculated using Eq. (2):

$$\text{area ratio} = \frac{\sum_{i=1}^{N} A_i}{S_{\text{total}}} \times 100\% \quad (2)$$

where A_i is the segmented area of the *i-th* truncated grain-tip region, N is the number of identified truncated regions, and S_{total} is the total analyzed area of the active wheel-end face.

Fig. 9 presents the stitched DIC micrographs of the end faces of the two CBN wheels before and after 40 min of truncation. One wheel was truncated in ambient air, whereas the other was truncated with oxygen supplied at 7.5 L/min under otherwise identical conditions. The individual micrographs were acquired using a 10× objective lens and stitched to cover the active wheel-end-face area. Before truncation, no flat-tip regions satisfying the image segmentation criterion were identified on either wheel. After truncation, the grain-tip truncation area ratios were 2.91% and 4.08% for the wheels processed in ambient air and with supplemental oxygen, respectively. Thus, the truncation area ratio measured with supplemental oxygen was 1.17 % or approximately 40% greater than that measured in ambient air. Although only one wheel was evaluated under each gas condition, this descriptive comparison indicates that supplemental oxygen was associated with a greater measured extent of grain-tip truncation under the tested conditions.

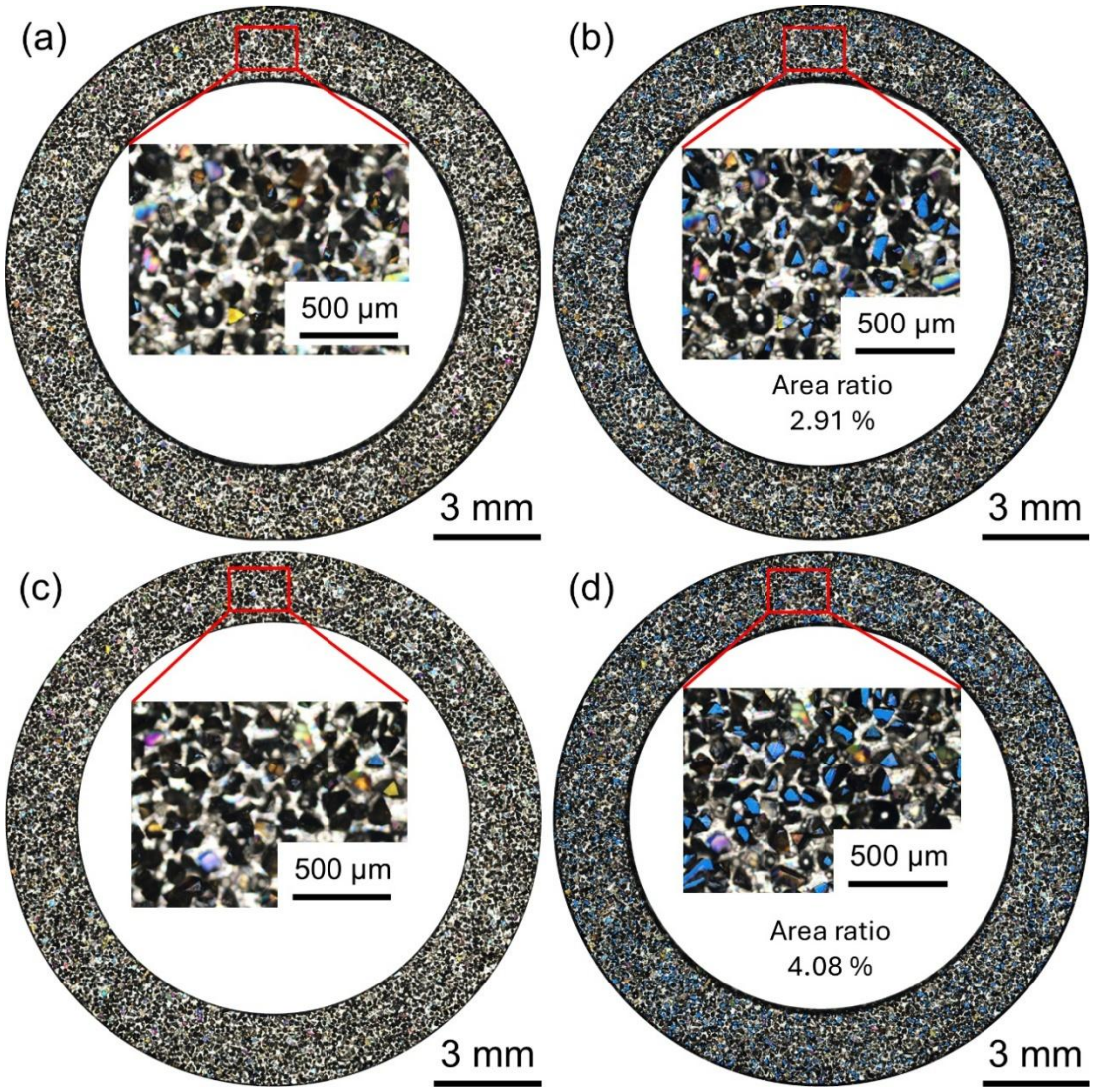


Fig. 9. DIC micrographs of the end face of the CBN grinding wheel before and after truncation in air and with oxygen supply.

Figs. 10(a) and (b) show the laser-microscope grain-height maps of the wheel before and after 40 min of truncation in ambient air, respectively. After truncation, the maximum grain protrusion height decreased, and locally flat regions were formed at the grain tips. Fig. 10(c) compares the corresponding height profiles extracted along the red lines in Figs. 10(a) and (b). The truncated grain tips retained relatively steep edge profiles, and no obvious profile discontinuities attributable to macroscopic grain fracture were observed. The grain-tip removal height was defined as the difference between the maximum heights of the corresponding profiles before and after truncation.

Based on this definition, the measured grain-tip removal height after 40 min of truncation in ambient air was 19.045 μm.

Figs. 10(d) and (e) show the grain-height maps of a separate wheel before and after 40 min of truncation with oxygen supplied at 7.5 L/min. Under the same load, rotational speed, and processing time as those used in ambient air, the wheel processed with supplemental oxygen exhibited a greater decrease in the maximum grain protrusion height and larger flat grain-tip regions. The corresponding profiles in Fig. 10(f) showed no obvious discontinuities attributable to macroscopic grain fracture. Together with the increase in truncation area ratio from 2.91% to 4.08%, these results indicate that supplemental oxygen was associated with a greater measured extent of grain-tip truncation under the tested conditions.

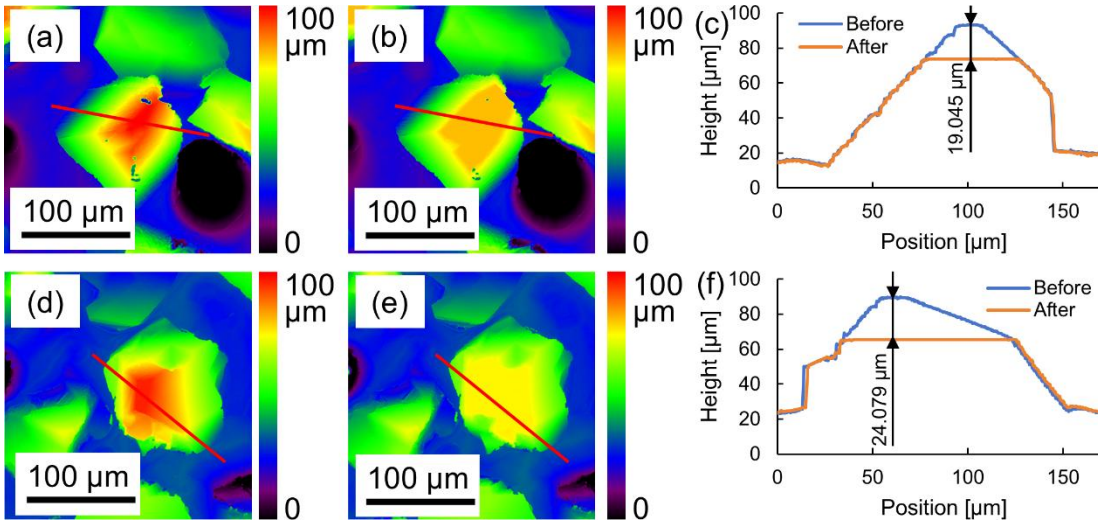


Fig. 10. CBN grain height maps and corresponding profiles before and after truncation: (a) before truncation in air, (b) after truncation in air, (c) height profiles in air, (d) before truncation with oxygen supply, (e) after truncation with oxygen supply, and (f) height profiles with oxygen supply

3.3. Surface generation by the truncated CBN wheel

Fig. 11 shows the effect of the feed per revolution on the surface topography of the GCr15 bearing steel ground using a truncated wheel with a truncation area ratio of

2.91%. At feed-per-revolution values of 50 and 30 μm/rev, the representative SWLI maps showed distinct feed-periodic grooves with spacings approximately corresponding to the respective feed-per-revolution values. The representative Sa values were 23.802 and 18.573 nm. At 10 μm/rev, the feed-periodic texture became less pronounced, and the representative Sa decreased to 7.026 nm, although a periodic surface pattern persisted. At 3 μm/rev, no distinct feed-periodic grooves were observed within the analyzed area, and the representative Sa decreased further to 3.149 nm. The progressive suppression of the feed-periodic texture with decreasing feed per revolution is consistent with the path-overlap mechanism illustrated in Fig. 4.

To characterize the spatial variation in surface roughness at each feed-per-revolution condition, Sa was measured at five randomly selected positions on the same ground surface. The points plotted in Fig. 11(e) represent the arithmetic means of these five spatial measurements, and the error bars extend from the minimum to the maximum measured values. Thus, the error bars characterize the within-surface spatial variation and do not represent the variability among independently repeated grinding tests.

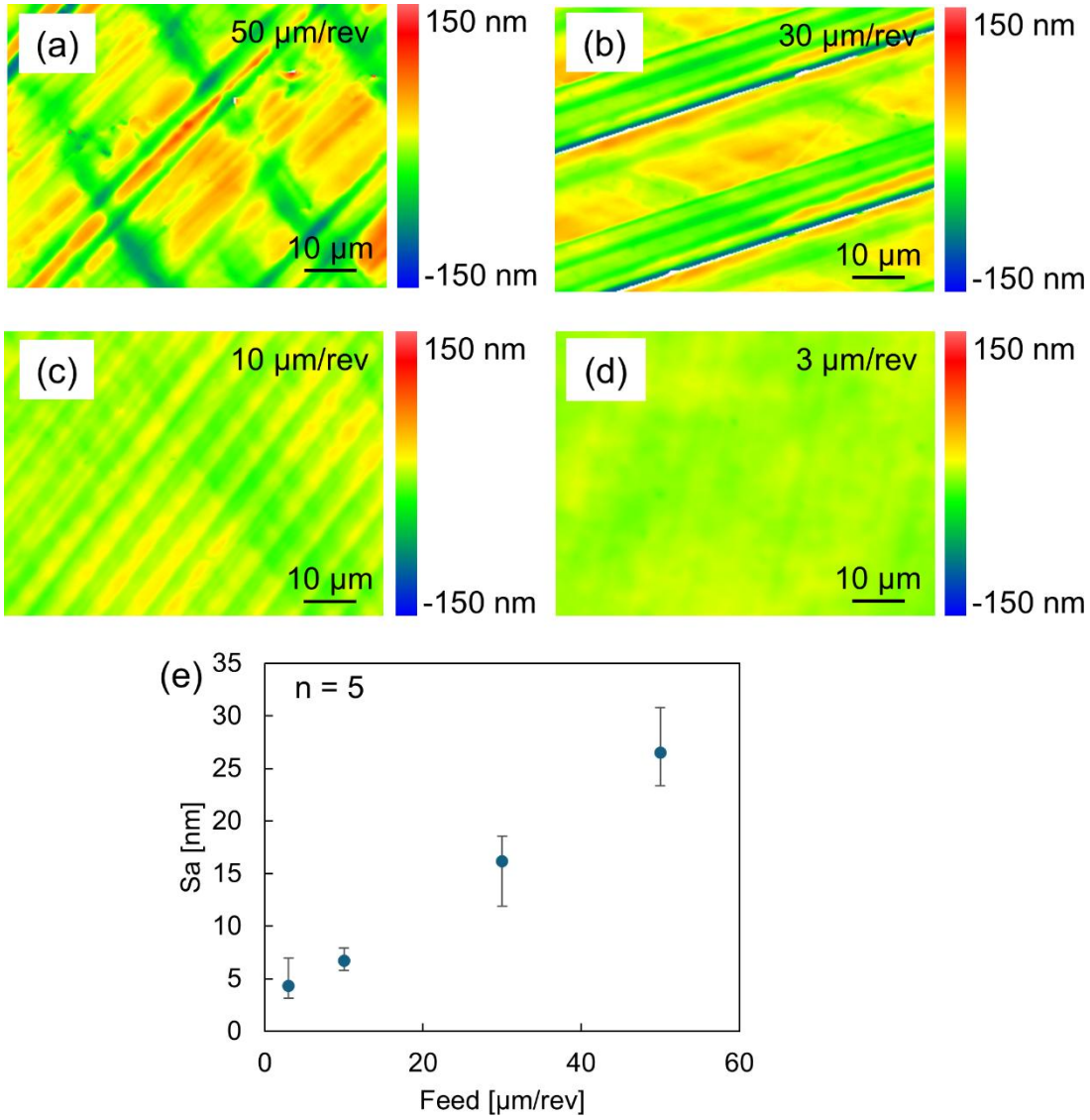


Fig. 11. Effect of feed per revolution on ground–surface roughness: ground surfaces obtained at feed per revolution values of (a) 50 μm/rev, (b) 30 μm/rev, (c) 10 μm/rev, and (d) 3 μm/rev, and (e) average Sa versus feed per revolution.

Fig. 12 compares the surface topographies produced using an untreated wheel and a truncated wheel under the same nominal ultra-smooth grinding conditions. The surface ground with the untreated wheel exhibited distinct grooves with Sa and Sz values of 10.996 and 153.041 nm, respectively. In contrast, no distinct grooves were

observed within the larger area measured using a 10× objective lens on the surface ground with the truncated wheel, for which Sa and Sz were 5.670 nm and 59.482 nm, respectively. This paired wheel comparison indicated that truncation was associated with the suppression of deep grooves and reductions in both Sa and Sz under the tested conditions.

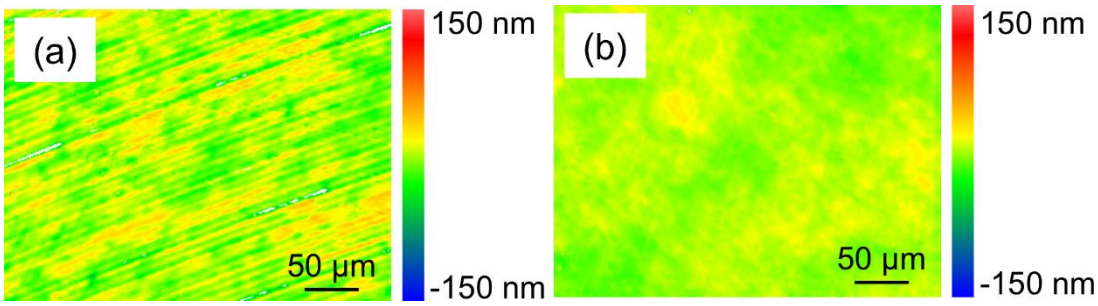


Fig. 12. Effect of wheel truncation on ground surface quality: surfaces ground using (a) an untreated CBN grinding wheel and (b) a truncated CBN grinding wheel.

Fig. 13 shows the effect of the nominal depth of cut on the surface topography of GCr15 bearing steel ground using a truncated wheel at a wheel rotational speed of 10,000 min^{-1} and a feed per revolution of 3 μm/rev. At a nominal depth of cut of 1 μm, the representative Sa and Sz values were 3.297 and 30.206 nm, respectively. As the nominal depth of cut increased from 3 to 15 μm, the surface undulations became more pronounced, and the representative Sa increased from 4.686 to 9.344 nm while remaining below 10 nm. Over the same range, the representative Sz values remained between 65 and 73 nm. Even at the substantially greater nominal depth of cut of 500 μm, the representative Sa and Sz values were 10.555 and 71.433 nm, respectively. Thus,

although surface roughness generally increased with the nominal depth of cut, a simple monotonic dependence was not observed over the entire range tested.

To evaluate the spatial variation in surface roughness at each nominal depth of cut, Sa was measured at five randomly selected positions on the same ground surface. The points plotted in Fig. 13(g) represent the arithmetic means of these five spatial measurements, and the error bars extend from the minimum to the maximum measured values. Therefore, the error bars characterize the within-surface spatial variation and do not represent the variability among independently repeated grinding tests.

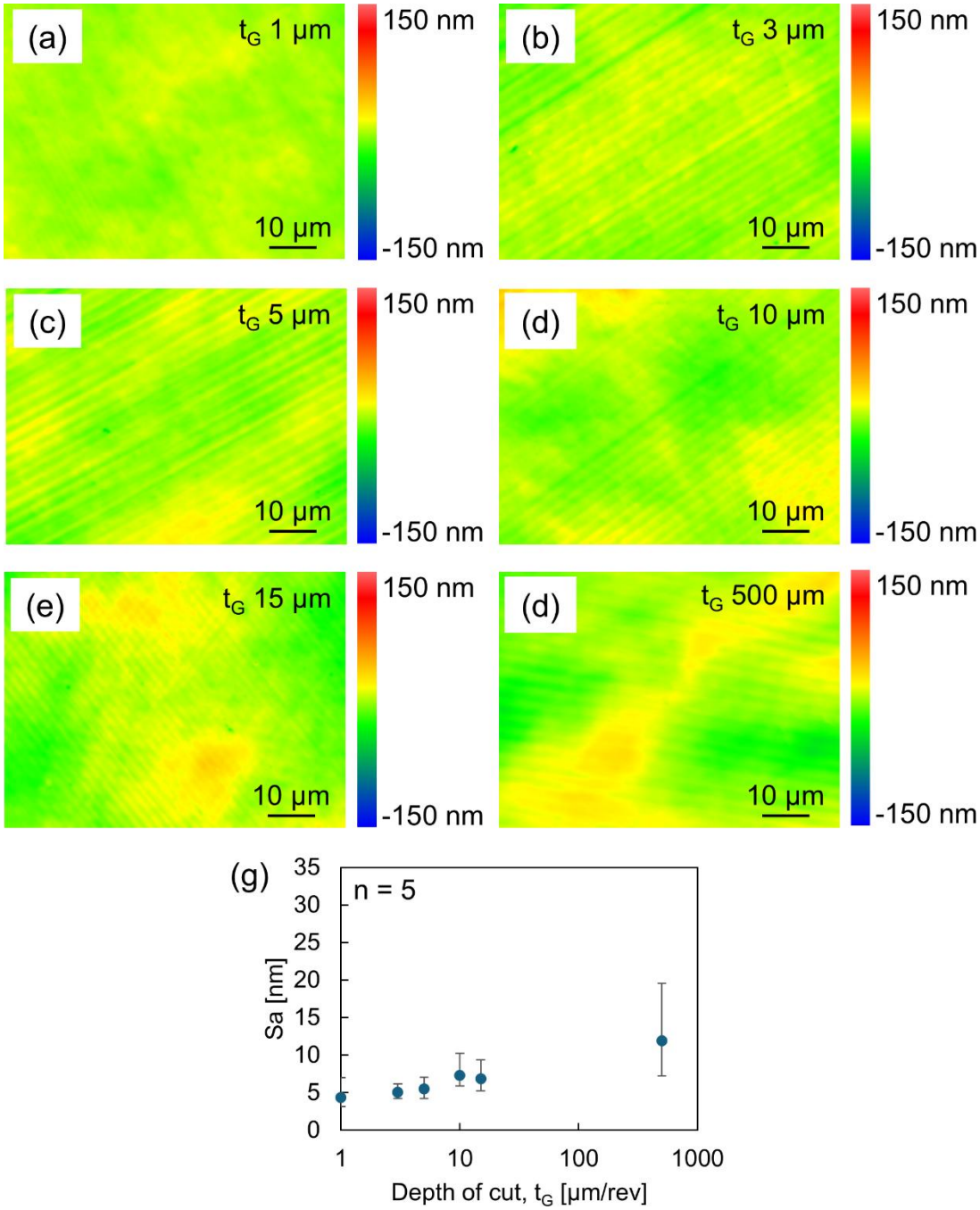


Fig. 13. Effect of depth of cut on ground surface roughness: (a–f) SWLI surface topographies obtained at depths of cut of 1, 3, 5, 10, 15, and 500 µm; (g) average Sa versus depth of cut on a logarithmic scale.

The surface obtained at a nominal depth of cut of 500 µm may be explained by the zone-specific material-removal mechanism schematically illustrated in Fig. 14. At a

small nominal depth of cut, the truncated grains on the wheel end face directly remove the residual surface irregularities. However, at a large nominal depth of cut, most of the material is presumed to be removed initially by the untruncated grains on the wheel periphery in the rough-grinding zone. The grains located along the rounded transition between the wheel periphery and end face then progressively reduce the residual height in the semi-finishing zone. Finally, the truncated grains on the wheel end face remove the remaining surface irregularities, while the overlap between adjacent grinding paths contributes to the generation of the finished surface.

According to this proposed mechanism, the nominal depth of cut of 500 μm does not correspond to the local engagement depth of the truncated end-face grains. Instead, most of the material is considered to have already been removed by the peripheral and transition-region grains before the workpiece engages with the truncated grains on the wheel end face. Consequently, the final surface roughness may be governed primarily by the flatness and height alignment of the truncated grain tips and the overlap between adjacent grinding paths, rather than directly by the nominal depth of cut. This zone-specific removal mechanism is consistent with the relatively smooth surface obtained at a nominal depth of cut of 500 μm under the present grinding conditions.

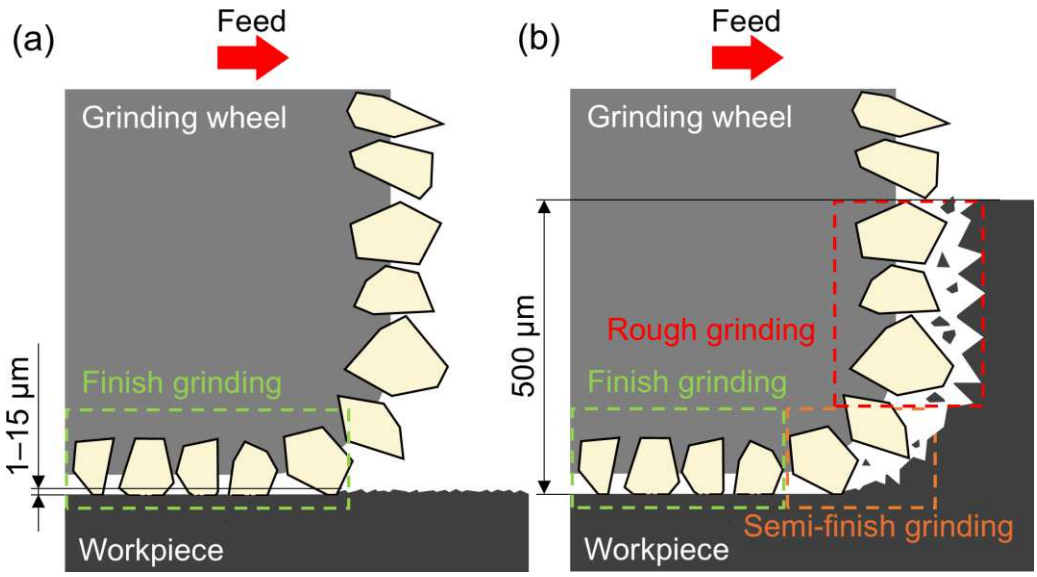


Fig. 14. Schematic of material removal during end-face ultra-smooth grinding with a truncated CBN wheel: (a) finish grinding at a small depth of cut and (b) zoned material removal at a 500 μm depth of cut.

3.4. Relationship between truncation extent and grinding performance

In the combined wheel-truncation and ultra-smooth-grinding process, the resulting surface characteristics were influenced by both the grinding parameters and the extent of wheel truncation. The grain-tip truncation area ratio was used as a quantitative measure of truncation extent and was defined as the percentage of the analyzed wheel-end-face area occupied by truncated grain-tip regions. To examine the relationship between truncation extent and workpiece surface roughness, an untreated wheel with a truncation area ratio of 0% and five truncated wheels with area ratios of 0.52%, 1.95%, 2.91%, 4.08%, and 5.07% were used to grind GCr15 bearing-steel specimens. The grinding conditions were a wheel rotational speed of 10,000 min^{-1}, a feed per revolution of 3 μm/rev, and a nominal depth of cut of 1 μm.

Fig. 15 shows the variation in the workpiece surface roughness with the grain-tip truncation area ratio. For each wheel, Sa and Sz were measured at five random positions on the same ground surface. The plotted values represent the arithmetic means of the five spatial measurements, and the lower and upper limits of the error bars indicate the minimum and maximum measured values, respectively. The mean Sa decreased as the truncation area ratio increased from 0% to approximately 3%. Among the wheels evaluated, the wheel with an area ratio of 2.91% produced the lowest mean Sa under the tested combination of grit size, workpiece material, and grinding conditions. At area ratios of approximately 4%–5%, both the mean Sa and its within-surface spatial variation increased markedly. These results indicate that excessive truncation may degrade the finished surface, despite increasing the total flattened grain-tip area. However, because each truncation area ratio was represented by a different wheel and the five measurements at each condition were spatial measurements on a single ground surface rather than independent wheel replicates, the results identified 2.91% as the best-performing area ratio among the wheels tested but did not establish a statistically validated optimum at approximately 3%.

As the grain-tip truncation area ratio increases, the total flattened grain-tip area increases, and a greater number of abrasive grains may simultaneously engage with the workpiece. The resulting increase in the effective wheel–workpiece contact area is expected to increase the normal grinding force. The associated increase in mechanical loading may destabilize the finishing action of the truncated grain tips and provides a

plausible explanation for the higher surface roughness observed at truncation area ratios above 2.91% in the present experiments. Thermal loading may also influence the grinding behavior; however, its contribution could not be evaluated because the grinding-zone temperature was not measured. Therefore, the appropriate extent of truncation is expected to depend on the wheel grit size, distribution of grain protrusion heights, workpiece material, and grinding conditions.

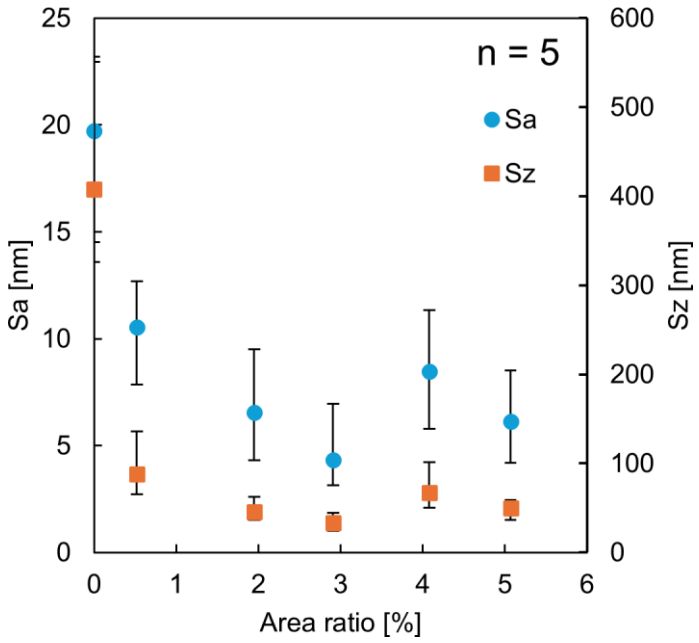


Fig. 15. Effect of truncation area ratio on the surface roughness of ground bearing-steel surfaces.

Fig. 16 shows the mean normal grinding force measured using wheels with different grain-tip truncation area ratios. The grinding-force signals were acquired using a multicomponent dynamometer at a sampling frequency of 1,000 Hz. In the present end-face grinding configuration, the z-direction force component, F_z, acted normal to

the ground surface. Accordingly, the normal grinding force plotted in Fig. 16 was defined as the time-averaged value of F_z. Each plotted value was calculated from 60,000 data points acquired over a 60 s interval during steady-state grinding. The measured normal grinding force increased with increasing truncation area ratio. This trend is consistent with the expected increases in the number of simultaneously engaged grains and the effective wheel–workpiece contact area as the total flattened grain-tip area increases.

A comparison of Figs. 15 and 16 suggests that increasing the truncation area ratio initially improves the surface finish by increasing the number of flattened grain tips. However, excessive truncation increases the normal grinding force and may consequently deteriorate the surface finish. Thus, the truncation area ratio should be controlled to achieve a balance between groove suppression and the grinding force. Because only one wheel was tested at each truncation area ratio, further tests using multiple wheels at each ratio are required to distinguish the effect of the truncation area ratio from the individual differences among wheels.

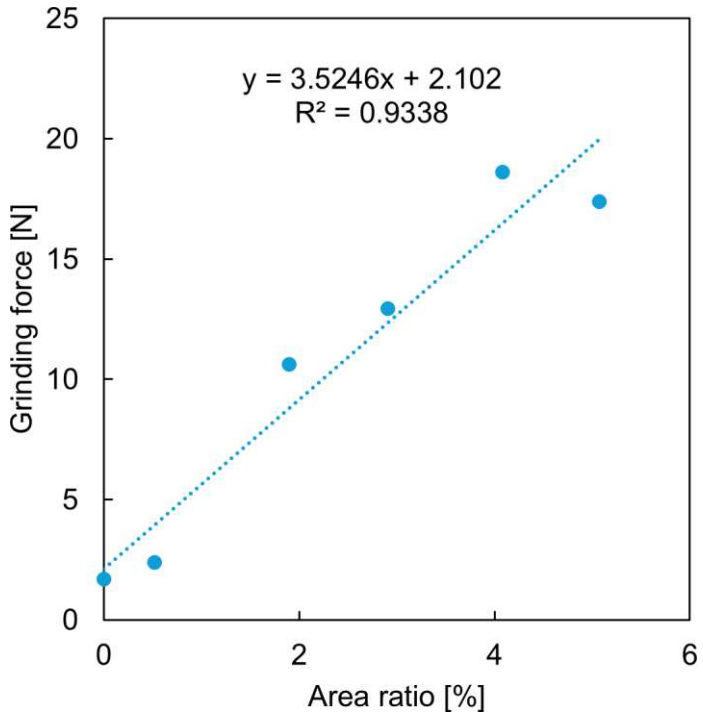


Fig. 16. Relationship between the truncation area ratio and grinding force during grinding with CBN wheels

4. Conclusion

This study investigated the oxygen-assisted truncation of coarse-grained electroplated CBN wheels and their application to the end-face ultra-smooth grinding of GCr15 bearing steel. The main conclusions are as follows:

1. The EPMA of the wear debris generated by friction between PCBN and quartz glass revealed a spatial association between B and O in the B-rich regions. Although the chemical states and phases of the reaction products were not identified, the observed elemental distributions were consistent with, but did not prove, an oxidative CBN removal mechanism. Under the tested wheel-truncation conditions, the grain-tip truncation area ratio was 2.91% in ambient air and 4.08%

with supplemental oxygen, while the corresponding measured grain-tip removal heights were 19.045 and 24.079 μm, respectively. These descriptive comparisons indicate that supplemental oxygen was associated with a greater measured extent of CBN grain-tip truncation during friction with quartz glass.

2. The truncated #120 electroplated CBN wheel produced a nanometer-scale surface roughness on GCr15 bearing steel. At a feed per revolution of 3 μm/rev, no distinct feed-periodic grooves were observed within the analyzed area, and an Sa value of 3.149 nm was obtained. Sa remained below 10 nm at nominal depths of cut ranging from 1 to 15 μm. Even at a nominal depth of cut of 500 μm, Sa and Sz were 10.555 and 71.433 nm, respectively. This result was consistent with the proposed zone-specific material-removal model, in which the peripheral and transition-region grains remove most of the material before the truncated end-face grains generate the finished surface.
3. The extent of grain-tip truncation was associated with changes in both surface roughness and normal grinding force. Among the wheels evaluated, the wheel with a truncation area ratio of 2.91% produced the lowest mean Sa under the tested grinding conditions. At higher truncation area ratios of approximately 4%–5%, increases in the mean Sa, its within-surface spatial variation, and the normal grinding force were observed. These results suggest that an intermediate truncation extent may provide a favorable balance between suppressing deep grooves and limiting the mechanical load during ultra-smooth grinding.

Overall, the results demonstrate the feasibility of combining oxygen-assisted wheel truncation with end-face grinding to generate nanometer-scale surfaces using a coarse-grained electroplated CBN wheel. Supplemental oxygen was associated with a greater extent of grain-tip truncation under the tested conditions, while the grinding results indicated that the truncation extent should be controlled to balance the surface finish and normal grinding force. Further experiments using independently prepared replicate wheels and direct chemical characterization of the wear products are required to

validate the observed relationships and clarify the oxygen-assisted CBN removal mechanism.

Acknowledgments

This work was supported by the Mazak Foundation, the Osawa Scientific Studies Grants Foundation, and the Advanced Machining Technology & Development Association.

Declarations

The authors have no relevant financial or non-financial interests to disclose.

All authors contributed to the study conception and design. Material preparation, data collection and analysis were performed by Qiushi Li. The first draft of the manuscript was written by Qiushi Li and revised by Qiushi Li and Akihisa Kubota. Mitsuru Murai and Koji Kawamura provided the experimental and measurement equipment. Funding acquisition was performed by Akihisa Kubota and Koji Kawamura. All authors read and approved the final manuscript.

References

[1] Jurko J, Panda A, Valíček J, Harničárová M, Pandová I (2016) Study on cone roller bearing surface roughness improvement and the effect of surface roughness on tapered roller bearing service life. Int J Adv Manuf Technol 82:1099–1106. https://doi.org/10.1007/s00170-015-7449-8

[2] Xia Z, Wu D, Zhang X, Wang J, Han E-H (2024) Rolling contact fatigue failure mechanism of bearing steel on different surface roughness levels under heavy load. Int J Fatigue 179:108042. https://doi.org/10.1016/j.ijfatigue.2023.108042

[3] Jang JY, Khonsari MM (2020) On the wear of dynamically-loaded engine bearings with provision for misalignment and surface roughness. Tribol Int 141:105919. https://doi.org/10.1016/j.triboint.2019.105919

[4] Xiao G, Jiang L, Peng W, Liu J, Deng C, Qian L (2022) Towards a deep understanding of oxidation in the material removal of GCr15 bearing steel during chemical mechanical polishing. Wear 508–509:204466. https://doi.org/10.1016/j.wear.2022.204466

[5] Dai Y, Meng F, Shi C, Wu C, Cao C, Li Z, Zhang Z (2026) Achieving near-atomic-level surface finish on GCr15 bearing steel via CMP: mechanisms and process optimization. Precis Eng 97:1019–1028. https://doi.org/10.1016/j.precisioneng.2025.11.018

[6] Kadivar M, Kitzig-Frank H, Azarhoushang B (2017) The effect of dressing parameters on the chip loading and ground surface quality by using grinding pins and grinding wheels with very fine grits. In: Fourth European Seminar on

Precision Optics Manufacturing. SPIE, 103260E. https://doi.org/10.1117/12.2272167

[7] Brinksmeier E, Mutlugünes Y, Klocke F, Aurich JC, Shore P, Ohmori H (2010) Ultra-precision grinding. CIRP Ann Manuf Technol 59:652–671. https://doi.org/10.1016/j.cirp.2010.05.001

[8] Denkena B, Krödel A, Wilckens M (2021) High performance peel grinding of steel shafts using coarse electroplated CBN grinding wheels. Prod Eng Res Devel 15:717–724. https://doi.org/10.1007/s11740-021-01047-1

[9] Wang H, Li X, Wang Z, Xu R (2020) Influence of electroplated CBN wheel wear on grinding surface morphology of powder metallurgy superalloy FGH96. Materials 13:1005. https://doi.org/10.3390/ma13041005

[10] Xia Y, Deng S, Wu M, Ni B (2024) Research on the grinding performance of an electroplated coarse-grained diamond grinding wheel by dressing. Machines 12:155. https://doi.org/10.3390/machines12030155

[11] Ichida Y (2016) Wheel life and cutting-edge wear in mirror-grinding using a coarse-grained cBN wheel treated by microdressing. Int J Autom Technol 10:753–758. https://doi.org/10.20965/ijat.2016.p0753

[12] Wu YB, Wang XY, Tachibana T, Kato M (2007) Laser truing and dressing of small vitrified CBN grinding wheel. Key Eng Mater 329:163–168. https://doi.org/10.4028/www.scientific.net/KEM.329.163

[13] Nomura M, Wu Y, Kuriyagawa T (2007) Investigation of internal ultrasonically assisted grinding of small holes: effect of ultrasonic vibration in truing and

dressing of small CBN grinding wheel. J Mech Sci Technol 21:1605–1611. https://doi.org/10.1007/BF03177382

[14] Guo B, Meng Q, Li S, Wu G, Xiang Y, Zhao Q (2022) Pulse laser precision truing of the V-shaped coarse-grained electroplating CBN grinding wheel. Mater Des 217:110650. https://doi.org/10.1016/j.matdes.2022.110650

[15] Zhao M, Qiu S, Li X, Wang K, Zhang W, Li L, Liu G, Zhang L, Liang SY (2026) Evolution of abrasive grain protrusion height in axial ultrasonic vibration-assisted grinding of CFRP with CBN grinding wheels. Compos Part B Eng 325:113930. https://doi.org/10.1016/j.compositesb.2026.113930

[16] Li Q, Kubota A, Murai M, Kawamura K (2025) Ultra-precision truncation of coarse-grained electroplated diamond grinding wheels using triboelectrically excited nitrogen. Diam Relat Mater 159:112815. https://doi.org/10.1016/j.diamond.2025.112815

[17] Touge N, Fujibayashi T, Miyamoto R, Sakamoto T, Kubota A, Touge M (2016) Development of quartz-truing technology for CBN electroplated wheels. J Jpn Soc Abras Technol 60:393–398. https://doi.org/10.11420/jsat.60.393

[18] Yasui H (2003) Development of polishingless ultra-smoothness grinding method (1st report): theory and some experimental investigations. J Jpn Soc Precis Eng 69:1713–1717. https://doi.org/10.2493/jjspe.69.1713

[19] Yasui H, Sakamoto R, Tanaka Y, Yamamoto Y, Sawa T (2008) Development of polishingless ultra-smoothness grinding method (3rd report): influence of normal feed. J Jpn Soc Precis Eng 74:1188–1192.

https://doi.org/10.2493/jjspe.74.1188

[20] Sakamoto R, Yasui H, Tanaka Y (2009) Development of polishingless ultra-smoothness grinding method (4th report): influence of parallel step feed. J Jpn Soc Precis Eng 75:768–772. https://doi.org/10.2493/jjspe.75.768